3B.3 USE OF VERTICALLY INTEGRATED ICE IN WRF-BASED FORECASTS OF LIGHTNING THREAT

Eugene W. McCaul, Jr.*, Universities Space Research Association, Huntsville, AL
Steven J. Goodman, NOAA/NESDIS/ORA, Silver Spring, MD

1. INTRODUCTION

As high-resolution numerical weather forecasts have become increasingly common, interest has grown in finding ways of exploiting the simulation data to produce accurate quantitative forecasts of lightning threat on the 0-6 h timescale. Much of the arlier work has emphasized statistical and climatological approaches to the problem, and has tended to focus on point forecasts (Mazany et al. 2002) or regional forecasts (Bright et al. 2004; Burrows et al. 2005; Bothwell 2005; Shafer and Fuelberg 2008). At the other end of the spectrum are sophisticated explicit cloud electrification schemes that can be added to a model (see, e.g., MacGorman et al. (2001), Mansell et al. (2002), and Kuhlman et al. (2006)).

In a previous conference, we presented preliminary findings (McCaul et al. 2006) regarding a new but relatively straightforward method of creating quantitative gridded lightning threat forecasts using various proxy fields from 2 km simulations of convective storm events made by the Weather Research and Forecasting (WRF, Skamarock et al. 2005) model. Early indications were that a proxy field based on the product of WRF updraft speed and graupel mixing ratio at the -15°C level showed considerable promise as a predictor of the threat, as measured by total lightning flash rate density. One of the limitations of this "graupel flux" method was that it relied heavily on behavior of storm updrafts, and thus could not by itself provide an accurate indication of the total areal coverage of the lightning threat.

In this paper, we present a new proxy field, the vertically integrated ice (VII) derived from the WRF hydrometeor fields, and show how it can be used in conjunction with the graupel flux to design a blended threat field that appears to be superior to either graupel flux or integrated ice alone. This VII field is the grid-column equivalent to storm total ice volume, and is found to correlate at least as well with total peak flash rate densities as did the graupel flux proxy. Both proxy fields are closely related to quantities found by other investigators (Cecil et al. 2005; Petersen et al. 2006) as being correlated with total flash rates in large databases of satellite-observed storms. These new methods thus have the advantage of being independent of convective regime, and are simpler to implement and less expensive to use than full cloud electrification routines applied to cloud-resolving models.

*Corresponding author address: E. W. McCaul, Jr., Universities Space Research Association, 6700 Odyssey Drive, Suite 203, Huntsville, AL 35806, e-mail: emccaul@usra.edu

2. METHODOLOGY

The methodology used in this work is similar to that employed in McCaul et al. (2006). For both the WRF proxy fields investigated here, we find the maximum gridded values achieved in a set of 7 carefully selected case study simulations, and compare them with the corresponding maximum values of similarly gridded lightning flash rate densities observed by the North Alabama Lightning Mapping Array (Rison et al. 1999; Krehbiel et al. 2000; Koshak et al. 2004; Goodman et al. 2005), for the same case study events. This technique is preferred over comparisons of simulations and observations at grid points, because of the widely recognized difficulty finescale models have at placing storms in exactly the right place at the right time. The case studies were chosen to reflect the variety of types of convective events that occur in the Tennessee Valley region of north Alabama, and includes warm season pulse storm events, squall lines, transitional season supercell outbreaks, and cold season post-frontal instability events.

For each proxy field, points were drawn on a scatterplot of simulated proxy peak value versus observed peak flash rate density, and regressions performed. In both cases, the regressions were statistically indistinguishable from linear relationships anchored at the origin, and thus our final linear regression calibration curves (not shown) were forced to pass through the origin. For the threat F_1 associated with graupel flux, the resulting calibration curve was:

$$F_1 = k_1 (w q_g)_m \tag{1}$$

where k_1 was found to be 0.042, w is the vertical velocity, q_g is the graupel mixing ratio, and the subscript m implies evaluation at the -15°C level in the mixed phase region. The interexperiment cross correlation between the simulated and observed data was 0.67 for this proxy, but the data points exhibit what appears to be greater variability relative to the regression line at the largest data values. This could suggest possible overprediction of graupel by WRF in the most intense storms, or perhaps a hint of nonlinear behavior in the calibration curve.

Likewise, for threat F_2 associated with VII, the calibration curve turned out to be:

$$F_2 = k_2 \int \rho (q_g + q_s + q_i) dz \tag{2}$$

where the vertical integral was performed over all the represented ice species, graupel q_g, snow q_s, and cloud

ice q_i, and the constant k_2 was 0.20. The interexperiment cross correlation between simulated and observed data for this threat was 0.83.

The WRF simulations used in this research were conducted on a 2 km x 2 km native grid centered on Huntsville, Alabama, initialized at either 00 UTC or 12 UTC on selected case study dates, and lasting 6-12 h. The model contained 51 levels on a constant 500 m vertical mesh. The time step used in the simulations was 12 s, and 25 history times were saved, at time intervals ranging from 15 min for the 6-h simulations, to 20 min for one of the longer simulations. The shorter 6-h simulations were used for cases where convection peaked shortly after model initialization, while the 12-h simulations were used for cases of afternoon summer storms that peaked more than 6-h after model initialization. In one case, we performed an 8-h simulation, with model saves taken at 20-min intervals. Model output was interpolated to a latitude-longitude grid with grid spacing of roughly 0.009 degrees, or about 1 km, for analysis and plotting. The WRF initial and boundary conditions came from ETA model analyses, with the addition of aircraft, METAR, and NWS Doppler radar velocity fields at t = 0. The WRF single moment, six-species microphysics (WSM6) package was used to represent clouds and their hydrometeors. This package allows simulation of only one large precipitating ice species, which we have characterized as graupel.

Both of our threats can be constructed and calibrated independently. Threat F_1 produces lightning flash rate density fields that appear reasonable, with peak values approximately matching those of LMA observations. Threat F_1 also exhibits temporal variability that reflects the growth and decay of individual simulated updraft pulses. However, the emphasis on storm updrafts necessarily limits the areal coverage of the lightning threat from F_1. Threat F_2 exhibits a footprint that has maxima nearly collocated with F_1, while covering a considerably larger area, because of its inclusion of storm anvil ice. Thus, F_2 can not only be calibrated against LMA flash density data, but can be forced, through truncation of the data at appropriately chosen lower bounds, to provide a close match for the areal coverage of observed lightning threat. On the other hand, F_2 is based on integrated quantities of hydrometeors, and thus tends to provide a threat field that does not display realistic temporal variability.

To obtain a blended threat parameter that performs well on both peak flash rate density and areal coverage, we construct threat F_3 as a linear weighted combination of F_1 and F_2:

$$F_3 = r_1 F_1 + r_2 F_2 \tag{3}$$

with the weights $r_1 = 0.95$ and $r_2 = 0.05$, based on results of sensitivity tests of the effects of various weight choices on resulting peak flash rate densities and areal coverages. A large weight for r_1 is desirable for proper representation of the observed temporal variations in lightning flash rate, but the weight r_2 should not be so small as to limit the clarity of rendition of threat areal coverage. The peak values of the blended threat F_3 remain properly calibrated, because both the input threats are calibrated and are approximately spatially and temporally coincident.

All our calibrations are done using LMA observations of gridded flash origin density. However, flash extent density is used to depict the lightning threat in our figures, because it highlights all the grid boxes visited by lightning flashes; the flash origin density field by itself is too sparse visually to be readily legible. Flash extent density is also a natural choice to use in our comparisons of threat areal coverage between the simulations and observations.

3. RESULTS AND DISCUSSION

We present several sample graphics for the 30 March 2002 supercell and squall line case described in McCaul et al. (2006). Another case (not shown) is also presented in the conference Powerpoint, and also in a formal manuscript that is currently in review.

Just after 0000 UTC on 30 March 2002, a strong cold front approached the Tennessee Valley and triggered a broken line of severe storms across Tennessee, with a small cluster of strong supercells breaking through a prefrontal capping inversion just south of the Tennessee River in northern Alabama. Values of convective available potential energy (CAPE) inferred from the WRF fields approached or exceeded 2000 J/kg across north Alabama. Just after 0400 UTC, one of the supercells produced a tornado near Albertville, Alabama. The supercells were strongly electrified, with overall total flash rates in excess of 60/min, as suggested by Fig. 1, a plot of LMA-derived gridded flash extent density (colors), along with NWS Doppler radar-derived low-level reflectivity (dBZ, grayshades) from 0400 UTC.

The WRF simulation initialized at 0000 UTC 30 March produced a broken line of strong storms across Tennessee, with a few isolated cells ahead of the main line. The simulated cells ahead of the broken line were not as strong as some of the cells in Tennessee, and were not exactly collocated with the observed Alabama supercells. By 0400 UTC, the WRF simulation contained strong cells, and the WRF-derived lightning threat based on graupel flux (Fig. 2) was widespread.

At 0400 UTC, the lightning threat based on vertically integrated ice (Fig. 3) is also widespread. Fig. 3 also shows the extent of the anvil ice field, which if not thresholded, would lead to overprediction of the areal coverage of lightning threat. Truncation of all VII-based threat values less than 0.4 flashes per 5 min per grid column yields an areal coverage in good agreement with LMA flash extent density coverage.

The blended threat derived from eq. (3) at 0400 UTC is given in Fig. 4. The net areal coverage, printed at the bottom center of the figure, is only slightly larger than the 15% observed. Note that neither peak flash

densities nor areal coverages are likely to match perfectly with observations, despite the calibration procedures and thresholding. This is because none of the data points in our calibration scatterplots lies exactly along their respective final regression lines.

It should be noted that our lightning threat algorithms produce areal threat coverage much more restricted and considerably more accurate than that provided by some traditional forecast parameters, such as CAPE. We have found that during the course of our simulations, the time-integrated areal coverage of lightning threat in our algorithm and in observations ranges from 10-30% for typical summertime pulse storm events, while CAPE is present over about 90% of the domain. For more organized frontal squall line cases, coverage of observed threat can increase to 50-80%, with CAPE coverage being often 90-100%.

The lightning threat products based on the simulations are promising, but not without limitations. While the model often produces storms at roughly the right time and location and intensity, it also sometimes produces unrealistically complex arrangements of storms, and excessive numbers of storms. This kind of error may be a reflection of the growth of errors that were present in the model initial state. The WRF model also has limitations with respect to the physics packages available at the time these simulations were conducted. WRF's WSM6 scheme, for example, does not have the capability of representing both graupel and hail simultaneously, and may overpredict graupel in certain circumstances. Caution should be used in applying these techniques to data from other models, or other configurations of the WRF model. The calibrations presented here are only strictly valid for the 2 km grid mesh and physics choices used in these simulations. For other models and other configurations, the calibrations should ideally be redone, or at least reasonable corrections applied.

4. SUMMARY AND OUTLOOK

The evidence suggests that these new approaches to lightning forecasting can be calibrated to yield accurate peak flash rate densities and total lightning areal coverage. These methods are also easy and inexpensive to implement, being based on simple post-processing operations on several of the standard model output fields.

Although the WRF simulations usually do a satisfactory job of generating deep convection in roughly the right places and times as observed, there are instances where the model exhibits phase errors in its positioning of convective storms or systems. Because no single control simulation is likely to be consistently accurate in its placement and timing of storms, it would be desirable to study the statistical characteristics of the combined threat fields derived from a diverse ensemble of WRF simulations. The combined output from such ensembles could be used to create envelopes of possible lightning threat, with contours of probability of exceedance of various flash rate densities.

There are other areas in which the WRF simulations could benefit from additional research and development. Perhaps the most significant involves improvement in the quality and accuracy of the initial and boundary condition fields. Assimilation of additional radar and satellite fields should be useful for this purpose. The model would also benefit from incorporation of higher moment ice microphysics schemes featuring additional hydrometeor categories. Finally, as computing power advances, routine use of finer model meshes than the 2 km mesh used here might also improve the fidelity of the representation of convective systems.

5. REFERENCES

Bothwell, P., 2005: Development of an operational statistical scheme to predict the location and intensity of lightning. *Preprints*, Conf. on Meteorol. Applications of Lightning Data, San Diego, CA, Amer. Meteor. Soc.

Bright, D. R., M. S. Wandishin, R. E. Jewell, and S. J. Weiss, 2004: A physically based parameter for lightning prediction and its calibration in ensemble forecasts. Preprints, 22nd Conf. Severe Local Storms, Hyannis, MA, Amer. Meteor. Soc., paper 4.3.

Burrows, W. R., C. Price, and L. J. Wilson, 2005: Warm season lightning probability prediction for Canada and the northern United States. Wea. Forecasting, 20, 971-988.

Cecil, D. J., S. J. Goodman, D. J. Boccippio, E. J. Zipser, and S. W. Nesbitt, 2005: Three years of TRMM precipitation features. Part I: Radar, radiometric, and lightning characteristics. Mon. Wea. Rev., 133, 543-566.

Goodman, S. J., R. Blakeslee, H. Christian, W. Koshak, J. Bailey, J. Hall, E. McCaul, D. Buechler, C. Darden, J. Burks, T. Bradshaw, and P. Gatlin, 2005: The North Alabama Lightning Mapping Array: Recent severe storm observations and future prospects. *Atmos. Res.*, **76**, 423–437.

Koshak, W. J., R. J. Solakiewicz, R. J. Blakeslee, S. J. Goodman, H. J. Christian, J. M. Hall, J. C. Bailey, E. P. Krider, M. G. Bateman, D. J. Boccippio, D. M. Mach, E. W. McCaul, M. F. Stewart, D. E. Buechler, W. A. Petersen, and D. J. Cecil, 2004: North Alabama Lightning Mapping Array (LMA): VHF source retrieval algorithm and error analyses. J. Atmos. Oceanic Technol., 21, 543-558.

Krehbiel, P.R., R.J. Thomas, W. Rison, T. Hamlin, J. Harlin, and M. Davis, 2000: GPS-based mapping system reveals lightning inside storms. EOS, 81, 21-25.

Kuhlman, K., C. Ziegler, E. Mansell, D. MacGorman, and J. Straka, 2006: Numerically simulated electrification and lightning of the 29 June 2000 STEPS supercell storm. *Mon. Wea. Rev.*, **134**, 2734–2757.

MacGorman, D. R., J. M. Straka, and C. L. Ziegler, 2001: A lightning parameterization for numerical cloud models. *J. Appl. Meteor.*, **40**, 459–478.

Mansell, E. R, D. R. MacGorman, C. L. Ziegler, and J. M. Straka, 2002: Simulated three-dimensional

branched lightning in a numerical thunderstorm model. *J. Geophys. Res.*, *107*, 4075, doi: 10.1029/2000JD000244.

Mazany, R. A., S. Businger, S. I. Gutman, and W. Roeder, 2002: A lightning prediction index that utilizes GPS integrated precipitable water vapor. Wea. Forecasting, 17, 1034-1047.

McCaul, E. W., Jr., K. LaCasse, S. J. Goodman, and D. Cecil, 2006: Use of high-resolution WRF simulations to forecast lightning threat. *Preprints*, 23rd Conf. Severe Local Storms, St. Louis, MO., paper 12.5.

Petersen, W. A., H. J. Christian, and S. A. Rutledge, 2005: TRMM observations of the global relationship between ice water content and lightning. Geophys. Res. Lett., 26 July 2005, vol. 32, no. 14, L14819 paper no. 10.1029/2005GL023236.

Rison, W., R. J. Thomas, P. R. Krehbiel, T. Hamlin, and J. Harlin, 1999: A GPS-based three-dimensional lightning mapping system: Initial observations in central New Mexico. Geophys. Res. Lett., 26, 3573-3576.

Shafer, P. E., and H. E. Fuelberg, 2008: A perfect prognosis scheme for forecasting warm season lightning over Florida. Part I: Model development. *Mon. Wea. Rev.*, **136**, 1817–1846.

Skamarock, W. C., J. B. Klemp, J. Dudhia, D. O. Gill, D. M. Barker, W. Wang, and J. G. Powers, 2005: A description of the Advanced Research WRF Version 2. NCAR Technical Note NCAR/TN-468+STR, 100 pp.

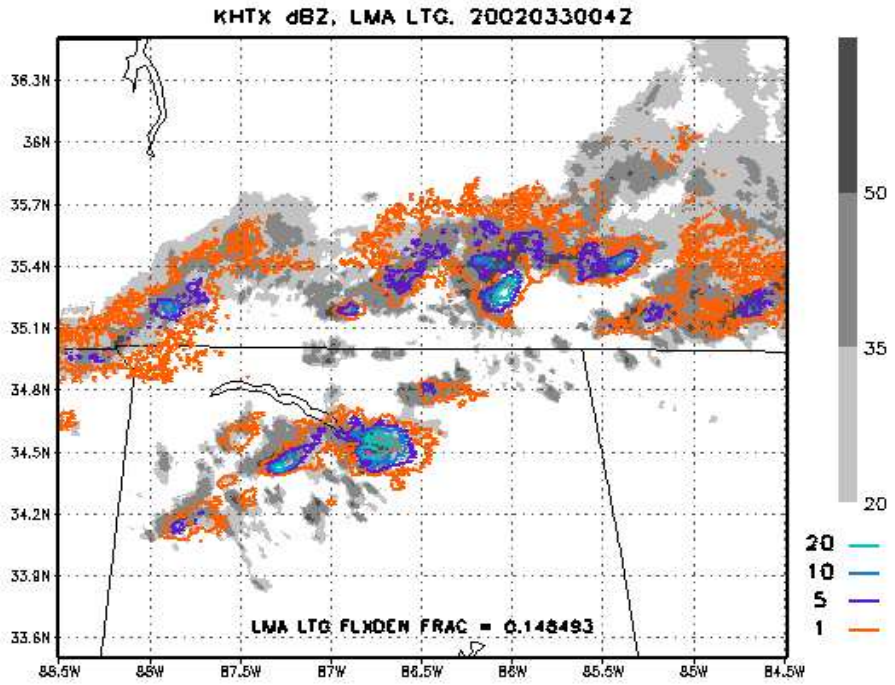

Fig. 1. LMA-derived gridded field of flash extent density (color contours) and radar-derived mid-level reflectivity (dBZ, grayshades) for 04 UTC 30 March 2002.

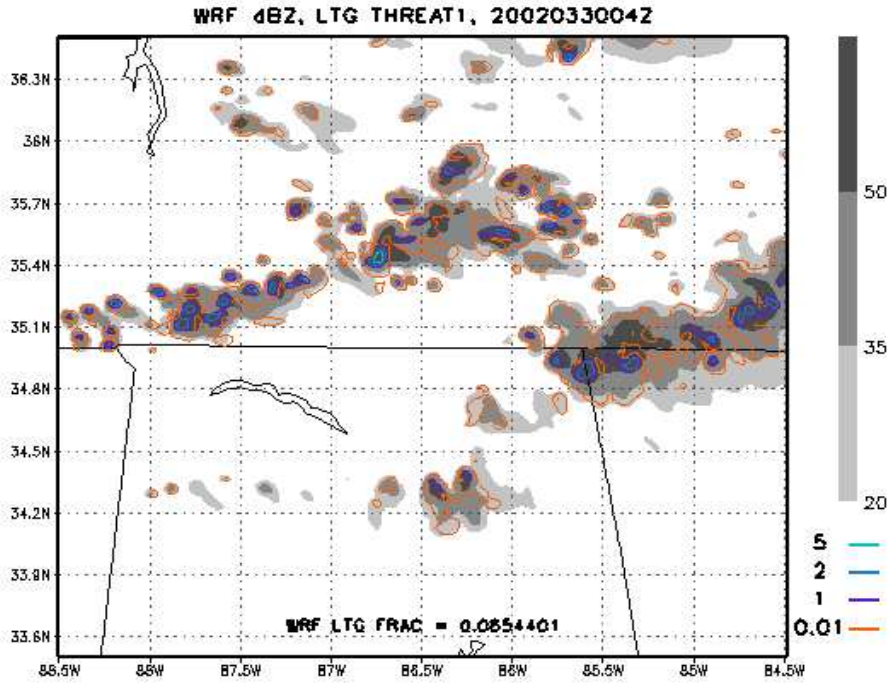

Fig. 2. Field of WRF-derived lightning threat (color contours) at 04 UTC on 30 March 2002, based on simulated graupel flux at the altitude where ambient temperature is -15° C. WRF reflectivity at that level is also shown (grayshades). Instantaneous areal coverage of predicted flash density is printed at the bottom of the figure.

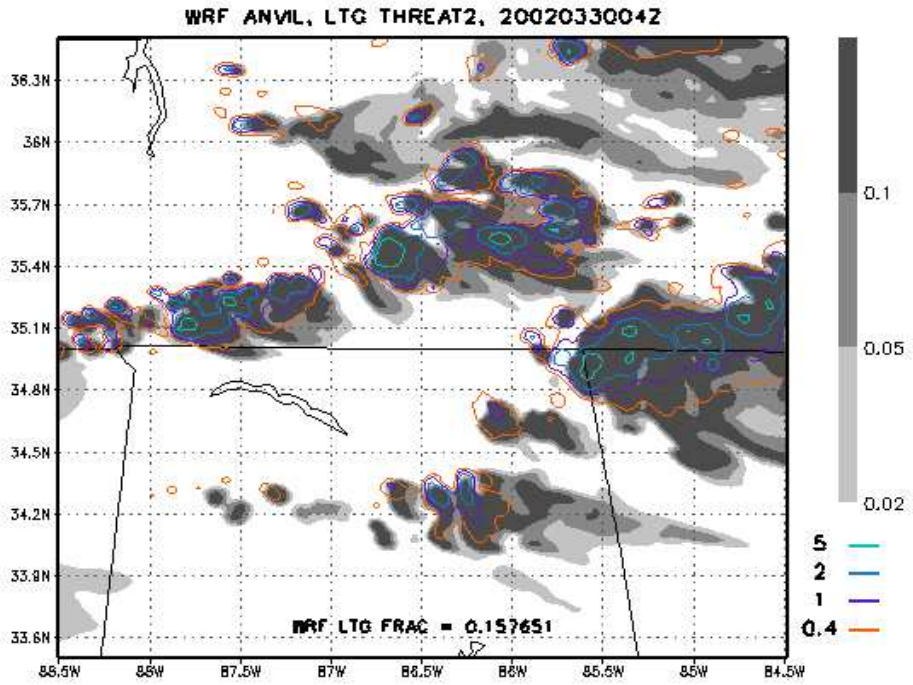

Fig. 3. Field of WRF-derived lightning threat (color contours) at 04 UTC on 30 March 2002, based on WRF vertically integrated ice. WRF anvil-level cloud ice field (grayshades) is also shown. Instantaneous areal coverage of predicted flash density is printed at the bottom of the figure.

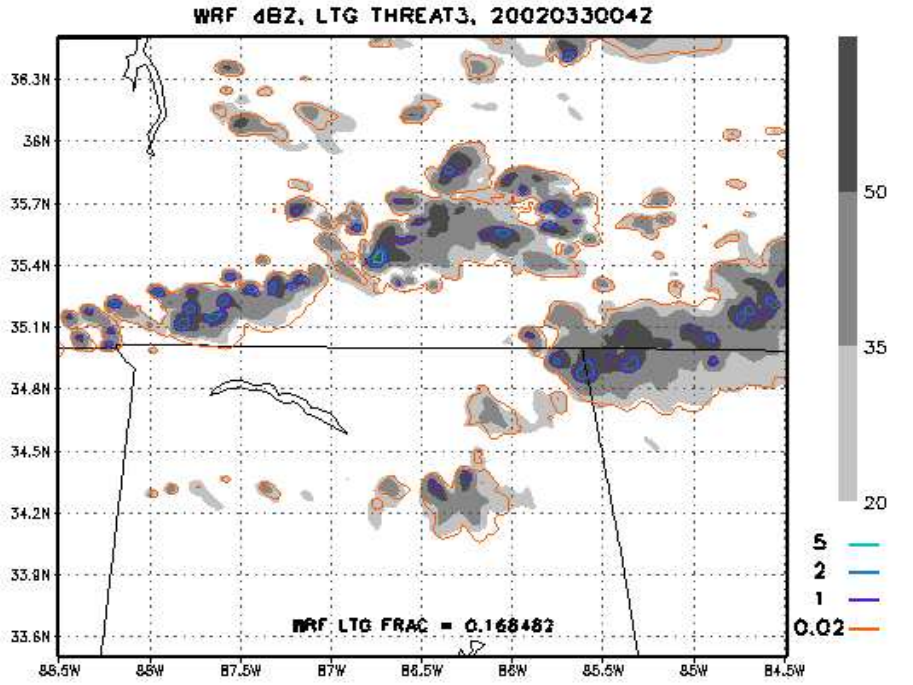

Fig. 4. Field of blended WRF-derived lightning threat (color contours) at 04 UTC on 30 March 2002, using the threats based on WRF graupel flux in Fig. 2 and vertically integrated ice in Fig. 3. WRF-derived midlevel reflectivity (dBZ, grayshades) is also shown. Instantaneous areal coverage of predicted flash density is printed at the bottom of

the figure.